J|A|C|S
ARTICLES
Published on Web 04/25/2006

On the Origin of the Unique Properties of Supported Au Nanoparticles

Mingshu Chen, Yun Cai, Zhen Yan, and D. Wayne Goodman*

Contribution from the Department of Chemistry, Texas A&M University, College Station, Texas 77842-3012

Received August 29, 2005; E-mail: goodman@mail.chem.tamu.edu

Abstract: The unique catalytic activity of supported Au nanoparticles has been ascribed to various effects including thickness/shape, the metal oxidation state, and support effects. Previously, we reported the synthesis of ordered Au monolayers and bilayers on TiO_x, with the latter being significantly more active for CO oxidation than the former. In the present study, the electronic and chemical properties of ordered monolayer and bilayer Au films have been characterized by infrared reflection adsorption spectroscopy using CO as a probe and ultraviolet photoemission spectroscopy. The Au overlayers are found to be electron-rich and to have significantly different electronic properties compared with bulk Au. The common structural features of ordered Au bilayers and Au bilayer nanoparticles on TiO_2(110) are described, and the exceptionally high catalytic activity of the Au bilayer structure related to its unique electronic properties.

1. Introduction

Nanoparticles exhibit distinct properties compared to their bulk counterparts and display catalytic activities critically dependent on particle size.[1−5] Highly dispersed Au particles have been shown to exhibit exceptional catalytic activity for several reactions.[1−10] Of these, low temperature CO oxidation has received the most attention experimentally and theoretically with the goal of understanding the origin of the extraordinary reactivity of Au nanoparticles.[1−8,11−24] Reports in the literature, however, vary widely, and the nature of the active Au species/structure/site remains obscure. It is generally accepted that the catalytic activity of Au depends to a large extent on the size of the Au particles; however other effects, such as the nature of the support, the Au−support interface, the particle shape, and metal−support charge transfer, are proposed to be of fundamental importance. Based on kinetic studies and scanning tunneling microscopic (STM) data, the most active structures of supported Au particles have been shown to be two atomic layers in thickness (a bilayer)[4,14] and to have distinctive electronic[25] and chemical properties[26,27] compared to bulk Au. Recently, we have synthesized two ordered Au films, a (1×1) monolayer and a (1×3) bilayer, that completely wet an ultrathin TiO_x film grown on Mo(112), i.e., TiO_x/Mo(112).[15,16] Recently STM has provided direct evidence for the wetting of the TiO_x/Mo(112) film by Au.[28] Unprecedented catalytic activity for CO oxidation was observed for the Au bilayer structure.[15] In this study, the electronic and chemical properties of the ordered Au films have been characterized by ultraviolet photoemission spectroscopy (UPS) and infrared reflection adsorption spectroscopy (IRAS) using CO as a probe. Structures for monolayer and bilayer Au nanoparticles on TiO_2(110) are proposed and compared to the Au (1×1) monolayer and (1×3) bilayer extended structures. The origins of the exceptionally high catalytic activity for the Au bilayer are explained in terms of the electronic charge on Au, the binding strength of the reactants, and limited dimensional effects.

2. Experimental Section

The experiments were carried out in three separate systems, each consisting of a combined elevated-pressure reactor and an ultrahigh vacuum (UHV) surface analysis chamber. The systems were equipped

(1) Haruta, M.; Yamada, N.; Kobayashi, T.; Iijima, S. *J. Catal.* **1989**, *115*, 301.
(2) Bell, A. T. *Science* **2003**, *299*, 1688.
(3) Rolison, D. R. *Science* **2003**, *299*, 1698.
(4) Valden, M.; Lai, X.; Goodman, D. W. *Science* **1998**, *281*, 1647.
(5) Biswas, P.; Wu, C. Y. *J. Air Waste Manage. Assoc.* **2005**, *55*, 708.
(6) Bond, G. C.; Thompson, D. T. *Catal. Rev.—Sci. Eng.* **1999**, *41*, 319.
(7) Haruta, A. *Chem. Rec.* **2003**, *3*, 75.
(8) Meyer, R.; Lemire, C.; Shaikhutdinov, Sh. K.; Freund, H. J. *Gold Bulletin* **2004**, *37*, 72.
(9) Hutchings, G. J. *Catal. Today* **2005**, *100*, 55.
(10) Daniel, M. C.; Astruc, D. *Chem. Rev.* **2004**, *104*, 293.
(11) Chen, M. S.; Goodman, D. W. *Catal. Today* **2006**, *111*, 22.
(12) Campbell, C. T.; Grant, A. W.; Starr, D. E.; Parker, S. C.; Bondzie, V. A. *Topics in Catalysis* **2001**, *14*, 43.
(13) Haruta, M.; Date, M. *Appl. Catal. A* **2001**, *222*, 427.
(14) Goodman, D. W. *J. Catal.* **2003**, *216*, 213.
(15) Chen, M. S.; Goodman, D. W. *Science* **2004**, *306*, 252.
(16) Campbell, C. T. *Science* **2004**, *306*, 234.
(17) Goodman, D. W. *Catal. Lett.* **2005**, *99*, 1.
(18) Lopez, N.; Janssens, T. V. W.; Clausen, B. S.; Xu, Y.; Mavrikakis, M.; Bligaard, T.; Norskov, J. K. *J. Catal.* **2004**, *223*, 232.
(19) Liu, Z. P.; Jenkins, S. J.; King, D. A. *Phys. Rev. Lett.* **2005**, *94*, 196102.
(20) Yang, J. H.; Henao, J. D.; Raphulu, M. C.; Wang, Y. M.; Caputo, T.; Groszek, A. J.; Kung, M. C.; Scurrell, M. S.; Miller, J. T.; Kung, H. H. *J. Phys. Chem. B* **2005**, *109*, 10319.
(21) Yan, W. F.; Chen, B.; Mahurin, S. M.; Schwartz, V.; Mullins, D. R.; Lupini, A. R.; Pennycook, S. J.; Dai, S.; Overbury, S. H. *J. Phys. Chem. B* **2005**, *109*, 10676.
(22) Shi, F.; Zhang, Q. H.; Ma, Y. B.; He, Y. D.; Deng, Y. Q. *J. Am. Chem. Soc.* **2005**, *127*, 4182.
(23) Diebold, U. *Surf. Sci.* **2005**, *578*, 1.
(24) Lee, S.; Fan, C. Y.; Wu, T. P.; Anderson, S. L. *Surf. Sci.* **2005**, *578*, 5.
(25) Chusuei, C.; Lai, X.; Luo, K.; Guo, Q.; Goodman, D. W. *Top. Catal.* **2001**, *14*, 71.
(26) Meier, D. C.; Goodman, D. W. *J. Am. Chem. Soc.* **2004**, *126*, 1892.
(27) Bondzie, V. A.; Parker, S. C.; Campbell, C. T. *Catal. Lett.* **1999**, *63*, 143.
(28) Chen, M. S.; Goodman, D. W., to be published.

10.1021/ja0557536 CCC: $33.50

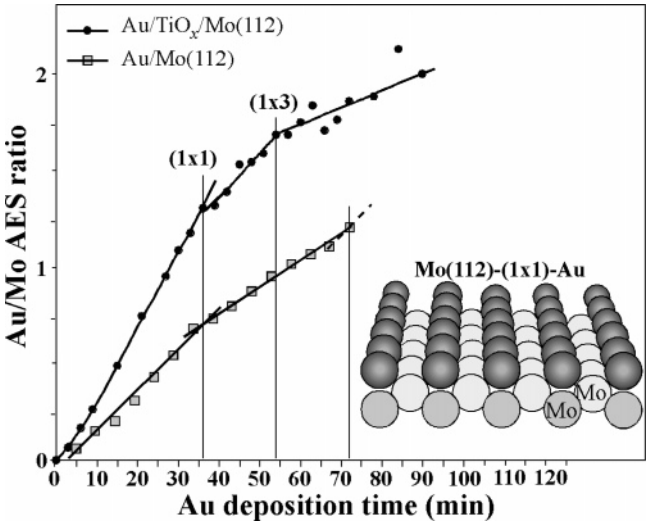

Figure 1. Plots of Au/Mo AES ratios versus deposition time. The insert is a structural model of (1 × 1)-Au/Mo(112).

with high-resolution electron energy loss spectroscopy (HREELS), polarization modulation IRAS (PM-IRAS), UPS, and metastable impact electron spectroscopy (MIES). Each chamber (base pressure of $\sim 10^{-10}$ Torr) is equipped with a cylindrical mirror analyzer for Auger electron spectroscopy (CMA-AES), low-energy electron diffraction (LEED), and a quadrupole mass analyzer. Kinetic measurements for CO oxidation were performed by transferring the sample *in situ* from the UHV preparation chamber into the reaction chamber through a double-stage, differentially pumped Teflon sliding seal. The Mo(112) sample was cleaned by repeated cycles of oxidation at 1200 K followed by a flash to 2100−2200 K and characterized using AES and LEED. The substrate temperature was measured via a (W/5 wt%Re)/(W/26 wt%Re) thermocouple spot-welded to the back sample surface. A liquid-nitrogen cryostat and an electron beam heater allowed control of the sample temperature between 90 and 2300 K.

The Mo(112)−(8 × 2)-TiO$_x$ support was prepared by depositing ~1 ML (ML, monolayer) of Ti from a filament source onto a Mo(112)−c(2 × 2)-[SiO$_4$] surface[29] which was then oxidized at 800 K and annealed at 1200 K (each step for 10 min in 5 × 10^{-8} Torr O_2). A subsequent anneal at 1400 K in 1 × 10^{-8} O_2 for an additional 5 min completely removed the c(2 × 2)-[SiO$_4$] film and any residual Si.[15,30] The TiO$_x$ film so prepared exhibits a sharp (8 × 2) LEED pattern and a single Ti−O phonon feature at 84 meV corresponding to the Ti−O stretching mode. This film synthesis is self-limiting in that different initial Ti coverages upon annealing yield a TiO$_x$ film with an identical Ti/Mo AES ratio corresponding to 1 ML. A possible structure for this film has been proposed,[15,30] where there are seven Ti atoms for every eight Mo atoms in the Mo(112) trough (the [−1−11] direction), with the Ti atoms bound to the surface via Ti−O−Mo bonds and to each other via Ti−O−Ti linkages. The oxidation state of Ti in the (8 × 2) film is 3+ as deduced from HREELS and XPS.[15,30] Au was deposited onto the Mo(112)−(8 × 2)-TiO$_x$ surface from a Au wire wrapped around a Ta filament that was heated resistively. The surface was then annealed at 900 K in O_2 of $<3 \times 10^{-9}$ Torr. The Au flux was calibrated using AES break points on Mo(112) and (8×2)-TiO$_x$/Mo(112) (see Figure 1). The Au coverage is reported in monolayers (ML) and referenced to the top layer Mo atom density in Mo(112). The order of the Au (1 × 1) and (1 × 3) structures were confirmed by sharp LEED patterns at Au coverages of ~1 and 1.3 ML, respectively (see Figure 1).

Research-grade CO was further purified by cooling to liquid N_2 temperature and then transferring to a glass bulb; O_2 was used as received. A CO/O_2 (2:1) mixture was used for the kinetic studies, and the CO_2 product was analyzed by mass spectrometry.

3. Results and Discussion

3.1. Electronic State of Catalytically Active Au. A number of theoretical and experimental studies have addressed the electronic properties of Au nanoparticles on oxide supports with the goal of understanding the unique properties of Au/TiO$_2$. Density functional (DFT) calculations suggest that the metal−support interaction alters the electronic structure of Au nanoclusters and promotes their catalytic activity for low-temperature CO oxidation.[31] In particular, defects on the oxide support are thought to play a key role in anchoring the Au particles and in transferring electron density to Au, with these two effects in combination contributing to the special catalytic activity.[4,18,32−38] Based on the shift of the Ti−O phonon mode in HREELS,[15] Ti was proposed to be oxidized from 3+ in the (8 × 2)-TiO$_x$/Mo-(112) to 4+ in the (1 × 1) and (1 × 3)-Au/TiO$_x$/Mo(112) upon bonding to Au. Oxidation of Ti in the support upon deposition of Au implies the formation of $Au^{\delta-}$.

In this study the vibrational stretching mode (ν_{CO}) of adsorbed CO was used to investigate the nature of the electronic state of Au in ordered Au films on TiO$_x$. The ν_{CO} mode shifts to lower frequency on electron-rich Au clusters and to higher frequency on electron-deficient clusters relative to bulk Au with the extent of this shift having been shown to correlate with the cluster charge.[39−41] The shift to lower frequency of the ν_{CO} has been purposed to arise from enhanced back-donation from the Au cluster to the antibonding $2\pi^*$ orbital of CO.[42] CO adsorption was carried out at 90 K with various CO exposures on the (1 × 1)-Au/TiO$_x$/Mo(112) surface and compared to the corresponding data for 1 ML Au on Mo(112) and 8 ML Au on Mo(112), hereafter referred to as (1 × 1)-Au/Mo(112) and Au(8L)/Mo-(112), respectively (Figure 2). Note that at coverages near 1 ML, Au on Mo(112) forms a (1 × 1) surface structure (see the insert of Figure 1) as deduced from the sharp LEED pattern. The arrangement of Au atoms in (1 × 1)-Au/Mo(112) is identical to the structure of Au in a (1 × 1)-Au/TiO$_x$/Mo(112) surface,[15] with the exception that in the former Au binds directly to the substrate Mo while in the latter, Au binds to the substrate through Ti. For low coverages of CO adsorbed on (1 × 1)-Au/TiO$_x$/Mo(112), a single ν_{CO} mode corresponding to CO on atop Au atom was observed at ~2107 cm^{-1} (Figure 2a). This feature

(29) Chen, M. S.; Santra, A. K.; Goodman, D. W. *Phys. Rev. B* **2004**, *69*, 155404.
(30) Chen, M. S.; Wallace, W. T.; Kumar, D.; Zhen, Y.; Gath, K. K.; Cai, Y.; Kuroda, Y.; Goodman, D. W. *Surf. Sci.* **2005**, *581*, L115.
(31) Rodriguez, J. A.; Liu, G.; Jirsak, T.; Hrbek, J.; Chang, Z. P.; Dvorak, J.; Maiti, A. *J. Am. Chem. Soc.* **2002**, *124*, 5242.
(32) Sanchez, A.; Abbet, S.; Heiz, U.; Schneider, W. D.; Häkkinen, H.; Barnett, R. N.; Landman, U. *J. Phys. Chem. A* **1999**, *103*, 9573.
(33) Lopez, N.; Norskov, J. K.; Janssens, T. V. W.; Carlsson, A.; Puig-Molina, A.; Clausen, B. S.; Grunwaldt, J. D. *J. Catal.* **2004**, *225*, 86.
(34) Mills, G.; Gordon, M. S.; Metiu, H. *J. Chem. Phys.* **2003**, *118*, 4198.
(35) Wahlstrom, E.; Lopez, N.; Schaub, R.; Thostrup, P.; Ronnau, A.; Africh, C.; Laegsgaard, E.; Norskov, J. K.; Besenbacher, F. *Phys. Rev. Lett.* **2003**, *90*, 026101.
(36) Okazaki, K.; Morikawa, Y.; Tanaka, S.; Tanaka, K.; Kohyama, M. *Phys. Rev. B* **2004**, *69*, 235404.
(37) Wang, Y.; Hwang, G. S. *Surf. Sci.* **2003**, *542*, 72.
(38) Yan, Z.; Chinta, S.; Mohamed, A. A.; Fackler, J. P., Jr.; Goodman, D. W. *J. Am. Chem. Soc.* **2005**, *127*, 1604.
(39) Guillemot, D.; Borovkov, V. Yu.; Kazansky, V. B.; Polisset-Thfoin, M.; Fraissard, J. *J. Chem. Soc., Faraday Trans.* **1997**, *93*, 3587.
(40) Ample, F.; Curulla, D.; Fuster, F.; Clotet, A.; Ricart, J. M. *Surf. Sci.* **2002**, *497*, 139.
(41) Yoon, B.; Häkkinen, H.; Landman, U.; Wörz, A. S.; Antonietti, J. M.; Abbet, S.; Judai, K.; Heiz, U. *Science* **2005**, *307*, 403.
(42) Häkkinen, H.; Abbet, S.; Sanchez, A.; Heiz, U.; Landman, U. *Angew. Chem., Int. Ed.* **2003**, *42*, 1297.

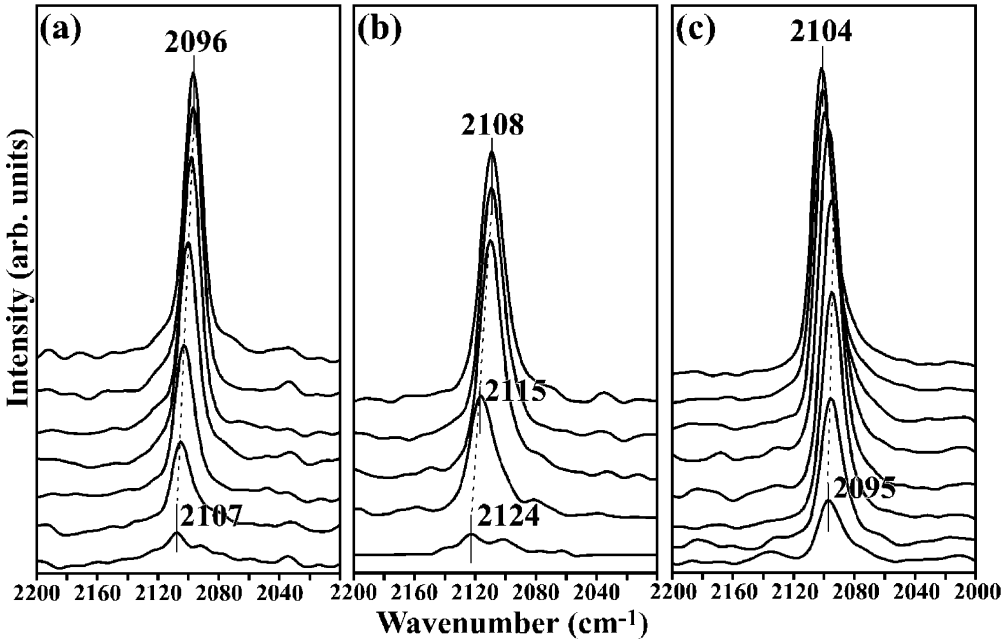

Figure 2. CO IRAS spectra on (a) (1 × 1)-Au/TiO_x/Mo(112), (b) Au(8ML)/Mo(112), and (c) (1 × 1)-Au/Mo(112) as a function of CO exposure at 90 K.

red-shifts to 2096 cm^{-1} as the CO coverage is increased to saturation, as seen with increasing CO coverage on Cu, Ag, and Au surfaces.[43−45] This red-shift is thought to occur because of limited back-donation from the Au d states into the $2\pi^*$ orbital of CO, with the Au−CO bonding occurring primarily through 5σ donation from CO to Au. A decrease in the extent of the 5σ donation to Au with increasing CO coverage leads to a red-shift in the CO mode.[26,44−47] As shown in Figure 2b, for CO adsorbed on multilayer Au, e.g., Au(8ML)/Mo(112), the ν_{CO} mode red-shifts from 2124 to 2108 cm^{-1} with increasing CO coverage. In contrast, on (1 × 1)-Au/Mo(112), the ν_{CO} mode remains essentially constant at 2095 cm^{-1} from low to relatively high (∼90%) CO coverages, finally blue-shifting to 2104 cm^{-1} at saturation. This blue-shift on (1 × 1)-Au/Mo(112) suggests more extensive back-donation between the Au d levels and the CO $2\pi^*$ antiorbital compared to bulk Au, consistent with a strong interaction between Au and the Mo substrate, and in agreement with previous UPS results for Au on Mo(110).[48,49]

The ν_{CO} frequency at low CO coverages then can be used to qualitatively estimate the charge on Au. As shown in Figure 2, the νCO frequencies occur at ∼2107, 2124, and 2095 cm^{-1} for low CO exposures on the (1 × 1)-Au/TiO_x/Mo(112), Au(8 ML)/Mo(112), and (1 × 1)-Au/Mo(112), respectively. These ν_{CO} frequencies indicate that the Au films on TiO_x/Mo(112) are electron-rich and that the extent of electron transfer from the substrate to the Au is less than the electron transfer to Au in (1 × 1)-Au/Mo(112). The extent of the charge transfer has been estimated to be ∼0.08 e from a Mo substrate to Au in Au/Mo(110).[48] Such charge transfer has been shown to be important in the bonding between dissimilar metals and to lead to relatively large perturbations of the metal electronic and chemical properties.[49,50] Furthermore, the differences between the frequency shifts as a function of CO coverage for (1 × 1)-Au/TiO_x/Mo(112) and (1 × 1)-Au/Mo(112) also suggest very little rehybridization of Au or charge transfer between Au and the Mo substrate in (1 × 1)-Au/TiO_x/Mo(112). This is likely a consequence of the absence of direct bonding between Au and Mo in (1 × 1)-Au/TiO_x/Mo(112), in contrast to (1 × 1)-Au/Mo(112).

The electron-rich nature of supported Au nanoparticles is supported by theoretical calculations[33,34] and ancillary experimental data.[4,35,36,38,51] Electron-rich Au nanoparticles are predicted to adsorb dioxygen more strongly and to activate the O−O bond via charge transfer from Au to form a superoxo-like species,[52] as well as facilitating the activation of CO.[18,32−34]

Figure 3 (left panel) shows a plot of the IR intensity of the CO feature versus CO pressure, where saturation of the IRAS signal corresponds to a saturation coverage of CO. The expression for a Langmuir isotherm (see insert of Figure 3) assumes nondissociative adsorption, a fixed number of adsorption sites, and an adsorption enthalpy independent of the coverage. The constant, b, in the expression is dependent on temperature (T) and the enthalpy/heat of adsorption (ΔH_{ads}), i.e., $b \propto \exp(\Delta H_{ads}/RT)$. Based on the Langmuir isotherm expression, the behavior indicated by the arrow in Figure 3 reflects an increase in b, corresponding either to an increase in the heat of adsorption at a given temperature or to a decrease in the temperature for a fixed set of adsorption conditions. The data of Figure 3 demonstrate that the order of the heats of adsorption for CO is (1 × 1)-Au/Mo(112) > (1 × 1)-Au/TiO_x/Mo(112) > Au(8ML)/Mo(112). This sequence is consistent with

(43) Dumas, P.; Tobin, R. G.; Richards, P. L. *Surf. Sci.* **1986**, *171*, 579.
(44) Bradshaw, A. M.; Pritchard, J. *Proc. R. Soc. London, Ser. A* **1970**, *316*, 169.
(45) France, J.; Hollins, P. *J. Electron Spectrosc. Relat. Phenom.* **1993**, *64*, 251.
(46) van Santen, R. A.; Neurock, M. *Catal. Rev. Sci. Eng.* **1995**, *37*, 557.
(47) Lemire, C.; Meyer, R.; Shaikhutdinov, Sh. K.; Freund, H. J. *Surf. Sci.* **2004**, *552*, 27.
(48) Rodriguez, J. A.; Kuhn, M. *Surf. Sci.* **1995**, *330*, L657.
(49) Rodriguez, J. A.; Campbell, R. A.; Goodman, D. W. *J. Phys. Chem.* **1991**, *95*, 5716.
(50) Rodriguez, J. A.; Goodman, D. W. *Science* **1992**, *257*, 897.
(51) Minato, T.; Susaki, T.; Shiraki, S.; Kato, H. S.; Kawai, M.; Aika, K. *Surf. Sci.* **2004**, *566*, 1012.
(52) Yoon, B.; Häkkinen, H.; Landman, U. *J. Phys. Chem. A* **2003**, *107*, 4066.

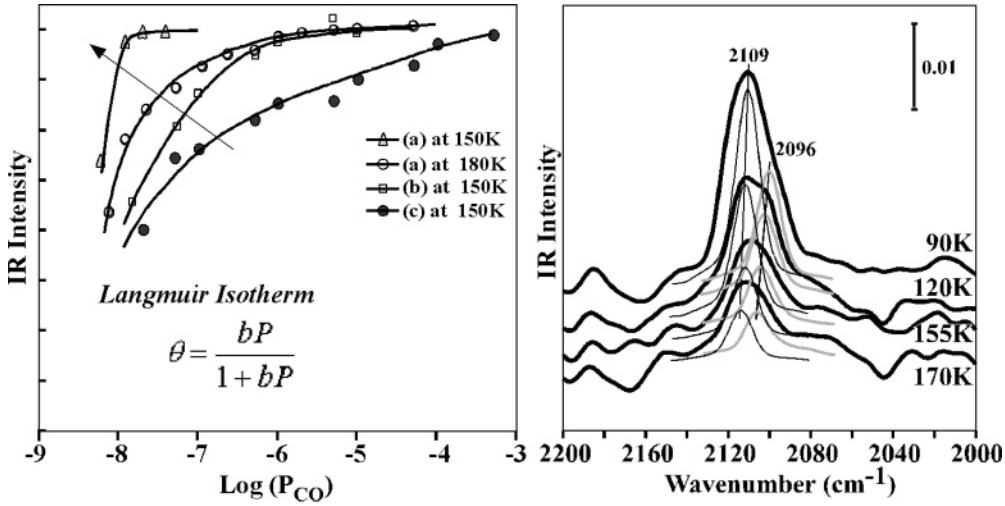

Figure 3. (Left panel) Isotherms from IRAS data of CO (from bottom to top) of (1 × 1)-Au/Mo(112), (1 × 1)-Au/TiO_x/Mo(112), and Au(8ML)/Mo(112). The maximum intensity is assumed to correspond to one monolayer CO coverage. The insert is an expression for a Langmuir isotherm where *b* is proportional to exp($\Delta H_{ads}/RT$). (Right panel) IRAS of CO on a (1 × 3)-Au/TiO_x/Mo(112) bilayer at various temperatures. The broad IRAS feature is decomposed into two features corresponding to atop CO on the bottom Au layer (low frequency one) and to atop CO on the top Au layer (high frequency one).

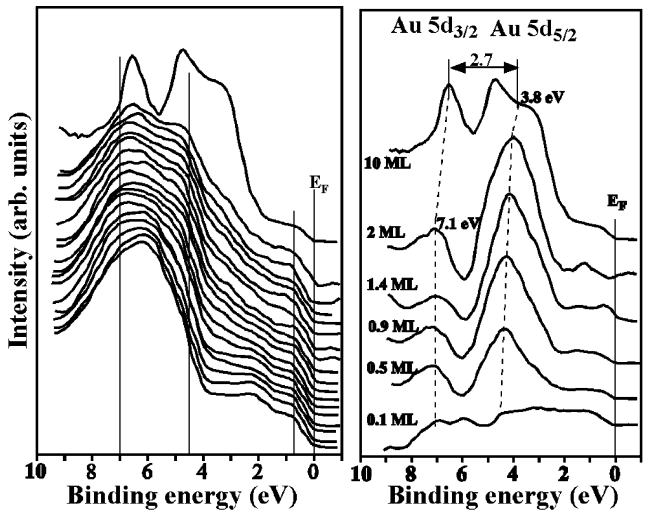

Figure 4. (Left panel) UPS data for Au on (8 × 2)-TiO_x/Mo(112) at Au coverages from 0 to 1.5 ML in increments of 0.1 ML, then one at 2 ML; the top spectrum shows the UPS for multilayer (~10 ML) Au. (Right panel) Difference spectra obtained by subtracting the contributions of the Mo substrate from the spectra in the left panel.

the shift of the observed ν_{CO} (see Figure 2) and also with electron-rich Au.

In (1 × 3)-Au/TiO_x/Mo(112),[15] both layers of Au are accessible to the adsorbate. CO adsorbed on this surface at 90 K yields a broad feature at ~2109 cm^{-1} (see Figure 3, right panel) that can be qualitatively decomposed into two features, one high frequency feature, assigned to atop CO bonded to the topmost Au atoms, and one low frequency feature assigned to CO bonded to the bottom layer Au atoms. Upon warming the sample to 120, then to 155, and finally to 170 K, the IR intensity of the mode corresponding to CO adsorbed on the topmost layer decreases more rapidly than that for the bottom layer. These results indicate that CO binds more tightly to the bottom Au layer than to the topmost Au layer.

The evolution of the valence band of Au evaporated on (8 × 2)-TiO_x/Mo(112) after an anneal at 900 K is shown in Figure 4. The spectrum of the TiO_x/Mo(112) substrate is shown at the bottom of the left panel. Upon deposition of Au, new valence band features appear at 4−5 and ~7 eV, corresponding to the Au $5d_{5/2}$ and Au $5d_{3/2}$ states, respectively, increasing in intensity with increasing Au coverage. Au on the TiO_x/Mo(112) grows epitaxially to 1.0 ML, forming a (1 × 1) monolayer at 1 ML, a (1 × 3) bilayer at 1.3 ML, then forms 3-D clusters at coverages > 1.3 ML.[15] Since the valence band features of Au films overlap with the features from the TiO_x/Mo(112), the unique features for the Au overlayers are more obvious in the difference spectra shown in the right panel of Figure 4. The Au $5d_{5/2}$ and Au $5d_{3/2}$ features are well-resolved at Au coverages below 2 ML. With increasing Au coverage, the $5d_{5/2}$ feature moves slightly toward the Fermi edge, while the $5d_{3/2}$ feature remains essentially unchanged. A spectrum of multilayer Au (~10 ML), i.e., metallic Au, is displayed at the top of both panels. The significant difference in the valence band spectrum for Au/TiO_x/Mo(112) compared with bulk Au indicates a strong redistribution of the Au 5d valence states in the formation of Au thin films on the oxide surface. Such redistribution has been observed for Au on SiO_2/Si and for Au on yttria-stabilized ZrO_2(100) with decreasing Au cluster size.[53−55]

3.2. Structure of Catalytically Active Au. Next we address the catalytic activity of the ordered (1 × 3)-Au/TiO_x/Mo(112) bilayer[15] (see the schematic structures in Figure 5a and 5b) and compare this activity with that of supported Au bilayer nanoparticles on TiO_2(110).[4] Au bilayer nanoparticles have been shown to exhibit higher catalytic activities for CO oxidation compared to Au monolayer or multilayer nanoparticles on TiO_2-(110). STM images acquired from a surface at low Au coverages show that Au forms one-dimensional (1-D) and two-dimensional (2-D) clusters with Au atom rows growing along the [001] direction of TiO_2(110) (schematically shown in Figure 5c).[4] After becoming thicker than one monolayer, the Au rows of the topmost surface cannot be atomically resolved with STM. Each row of Au in 2-D clusters are bound to five-fold coordinated Ti in TiO_2(110) and separated by a row of bridged-bonded oxygen atoms. Accordingly, the structure of the Au

(53) Zafeiratos, S.; Kennou, S. *Surf. Sci.* **1999**, *443*, 238.
(54) Guczi, L.; Petö, G.; Beck, A.; Frey, K.; Geszti, O.; Molnár, G.; Daróczi, C. *J. Am. Chem. Soc.* **2003**, *125*, 4332.
(55) Petö, G.; Molnár, G. L.; Paszti, Z.; Geszti, O.; Beck, A.; Guczi, L. *Mater. Sci. Eng., C* **2002**, *19*, 95.

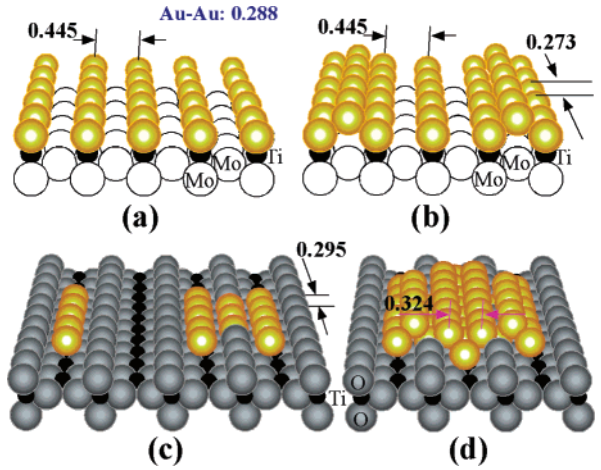

Figure 5. Structural models for (a) (1 × 1)-Au/TiO_x/Mo(112), (b) (1 × 3)-Au/TiO_x/Mo(112), (c) 1-D and 2-D Au clusters on TiO_2(110), and (d) a Au cluster two atomic layers in thickness on TiO_2(110). The oxygen atoms in the structural model of (a) and (b) are omitted for clarity.

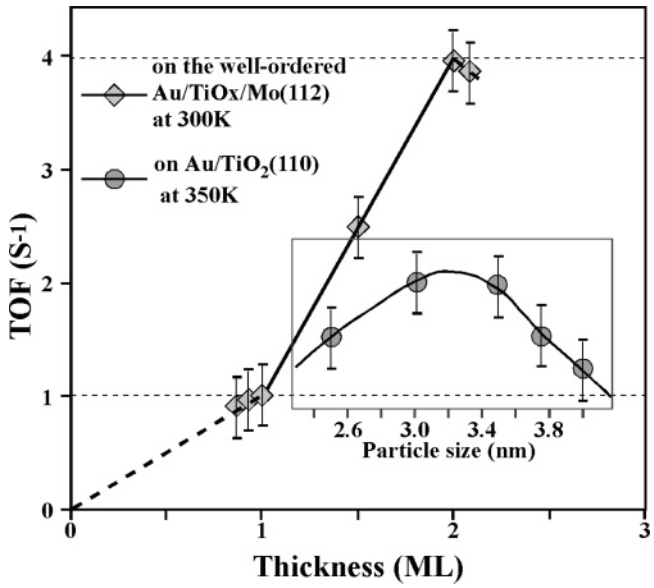

Figure 6. Activity for CO oxidation on supported Au catalysts. Data for the ordered Au films were taken from ref 15; those for Au/TiO_2(110) are from ref 4.

atoms in the first layer on TiO_2(110) is defined by the arrangements of the O and Ti atoms within TiO_2(110). This resulting structure is a 1-D chain-like structure with Au bound to five-fold coordinated Ti atoms and separated from each other by bridge-bonding oxygens (schematically shown in Figure 5c). Two of the Au rows may connect to form 2-D structures via Au atoms bound to oxygen vacancies (Figure 5c). It is likely that Au atoms in the top Au layer of the bilayer nanoparticles are pseudomorphic with respect to the bottom Au layer (see Figure 5d). Although an fcc(111) close-packed arrangement permits higher coordination within the top layer, the interactions between the bottom and top layer are believed to be weaker than between the atoms in bulk Au due to strain. Given these considerations, a likely arrangement of Au bilayer nanoparticles is shown in Figure 5d. In this structure the Au atoms in the top layer form 1D rows on the bottom layer Au atoms situated either on five-fold coordinated Ti or on oxygen vacancies and likely also bonded to bridging oxygen atoms. This structure compares closely with the (1 × 3)-Au/TiO_x/Mo(112) bilayer structure (Figure 5b). It is noteworthy that the top and bottom layers of Au atoms in the (1 × 3) bilayer are all accessible to the reactants, whereas, for the Au bilayer nanoparticles on TiO_2(110), only the top layer atoms and the edge sites of the bottom layer are accessible (see the structures of Figure 5b and 5d). This may account for the higher CO_2 activity for the (1 × 3) bilayer compared to Au bilayer nanoparticles on TiO_2(110) (see Figure 6) and is consistent with a synergistic reaction site for CO oxidation composed of atoms in the top and bottom layers of supported bilayer particles and at the edge sites of the bottom two Au layers in supported 3-D Au nanoparticles.

3.3. Origin of the Unique Catalytic Activity of Au. A unique feature of supported Au catalysts is a sharp particle size dependence of the catalytic properties.[1,4,7,57] From current−voltage (*I*−*V*) measurements of scanning tunneling spectroscopy (STS) on Au nanoparticles with various sizes on TiO_2(110), a metal-to-nonmetal transition (band gap variations between 0 and 1.4 eV) is observed as the Au cluster size is reduced from 3.5 to 1.0 nm (from a 3D multilayer to a 2D monolayer); a band gap of 0.2−0.6 V was found for Au bilayer nanoparticles.[4] A similar band gap−particle size relation has also been reported for Pd on TiO_2(110).[56] Based on the variation of the band gap as a function of the particle size[4] and the significant difference of the valence band structure of the ordered Au thin films on TiO_x/Mo(112) compared with bulk Au (see Figure 4), early work in our laboratories concluded that the pronounced structure sensitivity of CO oxidation on Au/TiO_2 relates directly to limited size or quantum size effects.

Limited size or quantum size effects have been invoked to account for the unique properties of nanometer-scale metallic particles relative to the bulk.[58−60] The properties of small metallic particles have been predicted theoretically to depend sensitively on the number of electrons, i.e., even or odd,[61] manifested as tunneling between discrete electronic levels of single metal particles.[62] Quantum size effects including electron transfer at the interface between Au nanoparticles and an oxide support has been reviewed by Daniel et al.[63] and Chen.[64] Ag nanoparticles have been theoretically shown to exhibit three novel, size-dependent vibrational features compared to the bulk.[65] Conductance measurements on single Ag nanoparticles on Al_2O_3/NiAl(110) reveal a series of equidistant resonances near the Fermi level with a decreasing energy separation with increasing cluster size.[66] Novel quantized charge transfer is manifested by a series of discrete features with uneven spacings and a relatively large band gap for small Au nanoparticles (<1.6 nm).[64] Significant quantum size effects with respect to the electronic configuration and the vibrational modes were found for Au nanoparticles less than 4 nm using Au-197 Mossbauer

(56) Xu, C.; Lai, X.; Zajac, G. W.; Goodman, D. W. *Phys. Rev. B* **1997**, *56*, 13464.
(57) Claus, P.; Bruckner, A.; Mohr, C.; Hofmeister, H. *J. Am. Chem. Soc.* **2000**, *122*, 11430.
(58) Perenboom, J. A. A. A.; Wyder, P.; Meier, F. *Phys. Rep.* **1981**, *78*, 173.
(59) Halperin, W. P. *Rev. Mod. Phys.* **1986**, *58*, 533.
(60) Mulder, F. M.; Stegink, T. A.; Thiel, R. C.; Dejongh, L. J.; Schmid, G. *Nature* **1994**, *367*, 716.
(61) Kubo, R. J. *Phys. Soc. J.* **1962**, *17*, 975.
(62) Ralph, D. C.; Black, C. T.; Tinkham, M. *Phys. Rev. Lett.* **1995**, *74*, 3241.
(63) Daniel, M. C.; Astruc, D. *Chem. Rev.* **2004**, *104*, 293.
(64) Chen, S. W. *J. Electroanal. Chem.* **2004**, *574*, 153.
(65) Kara, A.; Rahman, T. S. *Phys. Rev. Lett.* **1998**, *81*, 1453.
(66) Nilius, N.; Kulawik, M.; Rust, H. P.; Freund, H. J. *Surf. Sci.* **2004**, *572*, 347.

spectroscopy.[67] Ligand-stabilized metal nanoclusters in the size range of 1−2 nm exhibit well pronounced quantum size behavior.[68] Quantum well states in 1-D atomic chains of Au and/or Pd on NiAl(110) were found to be aligned as free-electron-like bands.[69]

Quantum-size effects were also found to influence the thermodynamic properties of metallic nanoparticles,[70] the properties of superconductors,[71] and chemisorptive properties of nanosized materials.[18,26,27,33,34,47,72] Charge transfer for CO adsorption depends critically on the size of a Na quantum dot.[72] Particle size effects were found for CO adsorption on Au deposits supported on FeO(111) grown on Pt(111)[47] and for CO[26] and oxygen[27] on Au/TiO_2. Pronounced thickness-dependent variations in the oxidation rate induced by quantum-well states were observed for ordered films up to 15 atomic layers in thickness.[73] All these studies indicate significant quantum size effects on the electronic, chemical, and catalytic properties of metal nanoparticles.

Based on theoretical[18,33,34,74−76] and experimental studies,[77,78] low-coordination Au sites have been proposed to play a key role in defining the catalytic activity of Au nanoparticles. DFT calculations for small Au clusters by Metiu et al. showed that surface roughness rather than a band gap is more important in influencing the binding strength of CO to Au.[34,74] TPD and IR results for CO adsorption on Au vapor-deposited on a thin FeO-(111) film grown on a Pt(111) by Freund et al. indicate that the adsorption of CO is dependent primarily on cluster morphology.[78] This group attributed the observed particle size effects to the presence of highly uncoordinated Au atoms in very small particles rather than quantum size effects.[47]

Kinetic measurements on Au monolayer and bilayer structures on TiO_x/Mo(112) (see Figures 5 and 6) show that the Au bilayer is significantly more active than monolayer Au for CO oxidation at room temperature.[15] A comparison of the structures of the monolayer and bilayer structures (see Figure 5a and 5b) reveals that the top layer Au atoms in each structure have very similar low coordination geometries. The relatively low activity of the monolayer compared to the bilayer suggests that low coordinated sites in themselves are insufficient for enhanced catalytic activity for CO oxidation. The key to activity is the formation of a bilayer Au structure where charge polarization at the metal−oxide interface yields an electron-rich lower Au layer and a low-coordinated upper Au layer.

Clearly the support plays a key role in determining the unique catalytic activities of nanosized Au. The support stabilizes and defines the morphologies and electronic properties of Au nanoparticles.[4,15,18,25,27,31,35] The perimeter/contact area of the interface between the Au particles and the support has been proposed as a unique reaction site where reactants are activated.[13,19,79−81] The structural models of the two ordered Au monolayer and bilayer structures shown in Figure 5 show that the Ti^{n+} sites in TiO_x/Mo(112) are not assessable to the reactants, since each surface Ti site binds directly to a Au atom. The exceptionally high catalytic activities for CO oxidation observed on the ordered Au bilayer are more consistent then with a Au-only mechanism for CO oxidation. It should be noted, however, that under realistic catalytic reaction conditions, these ordered surfaces may restructure, exposing the TiO_x substrate to the reactants. Further *in situ* structural studies are required to address this critical question. In any case, a Au-only CO oxidation reaction pathway was recently shown by DFT calculations to have a similar activation energy (0.36−0.40 eV) as that involving the oxide support.[76]

4. Conclusions

The electronic and chemical properties of ordered Au monolayers and bilayers on TiO_x/Mo(112) were investigated by UPS and IRAS using CO as a probe. The Au monolayer and bilayer structures are shown to be significantly electron-rich relative to bulk Au. A comparison of planar bilayer surfaces with supported Au bilayer nanoparticles indicates that the exceptionally high catalytic activities for the well-ordered Au bilayer structure can be attributed primarily to limited-dimensional effects and to the low degree of coordination of the topmost Au atoms.

Acknowledgment. We gratefully acknowledge the support of this work by the Department of Energy, Office of Basic Energy Sciences, Division of Chemical Sciences, the Robert A. Welch Foundation, and Battelle Memorial Institute, Pacific Northwest Division under Grant No. DOE DE-AC06-76RL0-1830.

JA0557536

(67) Paulus, P. M.; Goossens, A.; Thiel, R. C.; van der Kraan, A. M.; Schmid, G.; de Jongh, L. J. *Phys. Rev. B* **2001**, *64*, 205418.
(68) Schmid, G. *Adv. Eng. Mater*. **2001**, *3*, 737.
(69) Nilius, N.; Wallis, T. M.; Ho, W. *J. Phys. Chem. B* **2004**, *108*, 14616.
(70) Volokitin, Y.; Sinzig, J.; de Jongh, L. J.; Schmid, G.; Vargaftik, M. N.; Moiseev, I. I. *Nature* **1996**, *384*, 621.
(71) Guo, Y.; Zhang, Y. F.; Bao, X. Y.; Han, T. Z.; Tang, Z.; Zhang, L. X.; Zhu, W. G.; Wang, E. G.; Niu, Q.; Qiu, Z. Q.; Jia, J. F.; Zhao, Z. X.; Xue, Q. K. *Science* **2004**, *306*, 1915.
(72) Lindberg, V.; Hellsing, B. *J. Phys. C* **2005**, *17*, S1075.
(73) Aballe, L.; Barinov, A.; Locatelli, A.; Heun, S.; Kiskinova, M. *Phys. Rev. Lett.* **2004**, *93*, 196103.
(74) Mills, G.; Gordon, M. S.; Metiu, H. *Chem. Phys. Lett.* **2002**, *359*, 493.
(75) Lopez, N.; Nørskov, J. K. *J. Am. Chem. Soc*. **2002**, *124*, 11262.
(76) Remediakis, I. N.; Lopez, N.; Norskov, J. K. *Angew. Chem., Int. Ed.* **2005**, *44*, 1824.
(77) Lemire, C.; Meyer, R.; Shaikhutdinov, S.; Freund, H.-J. *Angew. Chem., Int. Ed*. **2004**, *43*, 118.
(78) Shaikhutdinov, Sh. K.; Meyer, R.; Naschitski, M.; Baumer, M.; Freund, H.-J. *Catal. Lett*. **2003**, *86*, 211.
(79) Guczi, L.; Peto, G.; Beck, A.; Frey, K.; Geszti, O.; Molnar, G.; Daroczi, C. *J. Am. Chem. Soc.* **2003**, *125*, 4332.
(80) Pietron, J. J.; Stroud, R. M.; Rolison, D. R. *Nano Lett*. **2002**, *2*, 545.
(81) Molina, L. M.; Hammer, B. *Phys. Rev. Lett*. **2003**, *90*, 206102.